Removal efficiency of gaseous benzene using lanthanide-doped mesoporous titania

Thuy-Duong Nguyen-Phan, Myoung Bock Song, Eun Woo Shin*

School of Chemical Engineering and Bioengineering, University of Ulsan, Mugeo-dong, Nam-gu, Ulsan 680-749, South Korea

ARTICLE INFO

ABSTRACT

The adsorptive removal of benzene from cerium- and lanthanum-doped mesoporous TiO_2 adsorbents was performed in a continuous-flow, fixed-bed reactor. The influences of lanthanide content and adsorption temperature were investigated. The adsorption efficiency of benzene was remarkably promoted in the presence of lanthanide. The adsorption capacity for benzene increased with lanthanide dosage, which was attributed to the enhancement in a specific surface area. It was determined that 5 mol% rare earth metal was the optimal amount for the highest benzene-adsorption, irrespective of adsorption temperature. Furthermore, the drastic reduction of adsorption capacities at higher temperature implied that benzene molecules were weakly adsorbed to the adsorbents. Additionally, X-ray photoelectron spectroscopy showed a correlation between the adsorption behavior and the chemical properties of mesostructure materials, typically the interaction of surface hydroxyl groups and the π-electron of benzene, and the formation of σ-bonding and d-π^* back-donation between the adsorbent and gaseous adsorbate.

1. Introduction

In recent decades, indoor air pollution has received considerable attention due to the increased time spent by people in tightly-sealed commercial buildings and apartment blocks. Volatile organic compounds (VOCs) have been considered a main indoor air pollutant due to their adverse human health effects caused by toxicity. The United States Environmental Protection Agency (EPA) has found concentrations of organic matters in indoor air to be two to five times greater than those in the outdoor environment [1,2]. Among several harmful pollutants, benzene is the most toxic compound, which not only causes sick building syndrome (SBS) and sick house syndrome (SHS) but also is a well-known human carcinogen [3]. A series of intermediate signs and symptoms occur after long exposure, such as headaches, respiratory disease, irritation, dizziness, nausea, anemia, and leukemia. Additionally, with high benzene levels, damage to the liver, kidneys, reproductive organs, central nervous system, or even death can occur. The main sources of benzene emissions are environmental tobacco smoke, oil, carpet, paint supplies, construction materials, wall/floor finishings, heating or cooking equipment, and nearby vehicular emissions. Therefore, the elimination and strict regulation of low concentrations of benzene in the air, on the order of sub-parts per million (sub-ppm) or parts per billion (ppb), are a matter of urgent concern (30 μg m^{-3}—indoor

air quality (IAQ) standard of Korea), especially in the rapid development of urban cities.

In reality, numerous alternative technologies for a sustainable environment to quickly and economically remove VOCs or benzene from indoor air have been developed and are affordable, such as absorption, adsorption, condensation, bio-filtration, catalytic decomposition, incineration, and UV photo-catalytic oxidation [4,5]. Among them, the adsorption on a solid surface is considered the most efficient and simple process for low concentrations at ambient or rather low temperature [6,7]. The choice of suitable and potential adsorbents is not only crucial in determining the adsorption performance but also imperative in aspects of economy and technique. An adsorbent material should have the following properties: high internal volume and/or surface area for the accessibility of the adsorbate molecules, good mechanical and kinetic properties, inexpensive raw materials and methods for production [8]. The quantity of organic compounds bound to the adsorbent depends on several factors, including physico-chemical properties of the adsorbent, VOC structure or concentration, temperature, and the nature of adsorbent such as the adsorbate interaction and contact time.

For efficient application in gas adsorption, the use of porous materials as the adsorbent has been extensive because of several prominent properties [8]. There are various preferable synthetic adsorbents, including activated carbon [9,10], zeolite [11,12], silica [13–15] and alumina [16,17]. Since the first synthesis of mesoporous molecular sieves (M41S family) in 1992 by the Mobil Oil Company for petroleum refining purposes [18] and the development of different kinds of mesostructured silica, such as SBA-15 [19] and MCM-48

* Corresponding author. Tel.: +82 52 259 2253; fax: +82 52 259 1689.
  E-mail address: ewshin@mail.ulsan.ac.kr (E.W. Shin).

[20], ordered mesoporous materials with specific structural and chemical features have been very useful for adsorption processes [21–24]. Subsequently, extensions of mesoporous transition metal oxides by several methods to a wide variety of applications in different fields have attracted significant attention [25–27]. Metal-oxide mesostructures are more suitable for adsorption because they do not suffer from mass transfer limitations and therefore allow easier diffusion of reactants [28]. Indeed, due to low cost, low density, relatively low toxicity, high strength, excellent corrosion resistance, physical stability, and chemical stability, titanium oxide nanomaterials are playing an important role in solving serious environmental problems and other challenges [29]. Nevertheless, due to narrow pore diameters, small surface area, and thermal instability that lead to limited practical applications, mesoporous TiO_2 materials with well-defined pore structure, high anatase crystallinity, high surface-to-volume ratios, and more active sites have been well studied with or without a structure-directing agent [25,30–32]. Additionally, in order to improve the performance of mesoporous titania, several promising methods have been achieved, such as doping with metal/non-metal species, coupling with other semiconductor oxides or depositing nanoparticle noble metals [33,34]. Among them, the alteration in electronic properties/structures of materials, which are closely related to chemical composition, the atomic arrangement as well as the physical dimensions, due to suitable metal dopants, have been proven to be the most feasible and favorable methods [35–37]. The incorporation of doping metal into the mesoporous TiO_2 framework can provide several beneficial effects, including more adsorption sites or active sites on the surface or inside channel, combined with acidic points that are more efficient for adsorption because of the changes in physico-chemical and structural properties.

The aim of the current study is to utilize cerium- and lanthanum-doped mesoporous TiO_2 as benzene adsorbents and subsequently, the effect of two important factors, the doping content and adsorption temperature, on the adsorptivity of benzene were investigated. The adsorption capacity (q) evaluated from the breakthrough curve provides a measurement of the amount of adsorbate that reaches saturation on a particular material under certain conditions of temperature and concentration. Furthermore, the adsorption behavior is suggested to rely on either the physico-chemical properties of the adsorbents or the interactions between gaseous adsorbed benzene and porous materials.

2. Experimental

2.1. Adsorbents

A series of lanthanide-doped mesoporous TiO_2 were synthesized via a sol–gel method using dodecylamine as a structure-directing agent. The preparation procedures were described in detail elsewhere [38]. All materials were designated as xCe–TiO_2 and xLa–TiO_2, where x stands for mol% Ln (x = 0.1, 0.5, 1.0, 5.0 and 10) and the un-doped sample was named TiO_2. The adsorbents were characterized elsewhere by N_2 sorption measurements, field-emission scanning electron microscopy, powder X-ray diffraction and X-ray photoelectron spectroscopy.

2.2. Adsorption tests

The adsorption experiments were performed at 303 K in the continuous-flow, fixed-bed unit [24]. Prior to each test, 0.1 g of adsorbents were weighed into a 9-mm i.d. Pyrex U-shaped reactor and subsequently pretreated with a flow of nitrogen for 1 h at 523 K to remove humidity and carbonaceous matters on the surface. N_2 was used as a carrier with a constant flow rate of 100 ml min^{-1},

whereas 0.9 μl h^{-1} of liquid benzene was supplied by a micro-syringe pump with line heating at 323 K for phase transfer. The tests were additionally conducted at 343 K to survey the effect of temperature on the benzene adsorbability. Benzene quantities were recorded by a gas chromatograph Acme 6000 M GC (Young Lin instrument Co., Anyang, Kyoungki, South Korea) using a DB-WAX column held at 423 K and flame ionization detector (FID) at 473 K. Subsequently, the adsorption performance with reproducibility tests was obtained with breakthrough curves of gaseous benzene that were applied for adsorption capacity estimation.

3. Results and discussion

3.1. Characteristics of materials

The textural properties of all samples were investigated in the previous study [38] and are summarized in Table 1. In this report, the presence of rare earth metals increased the specific surface area, micropore area, total pore volume, and pore diameter, and suppressed the crystallite sizes in comparison with pure mesoporous titania. Among the different doping amounts, 5.0Ce–TiO_2 and 5.0La–TiO_2 samples possessed the highest nitrogen adsorbability and contrarily, the smallest anatase sizes. Moreover, complicated chemical states, such as $Ti^{2+/3+/4+}$, $Ce^{3+/4+}$, chemisorbed oxygen/hydroxyl groups and lattice oxygen (Ti–O, Ce–O and Ce–O–Ti) on the surface were observed for the cerium dopant, which was different than lanthanum doped samples (only La^{3+}). All the results were ascribed to the formation of Ti–O-rare earth element bonds and the Ln_xO_y lattice, the interaction between titanium species (tetrahedral and octahedral sites) or between Ti and individual dopant metals, combined with charge imbalance behaviors. Consequently, certain characteristics of the materials may make them efficient for heterogeneous reactions, typically in the adsorption reaction.

3.2. Influence of rare earth metal amounts on benzene removal efficacy

A series of benzene adsorptions were performed in a continuous gas flow reactor using cerium- and lanthanum-doped mesoporous titania. The adsorption capacities of benzene were calculated from the breakthrough curves that displayed the relationship between relative benzene concentration and adsorption time. Table 2 shows the influence of rare earth metal in mesoporous TiO_2 on benzene removal. The adsorption performances of benzene on mesoporous TiO_2, cerium- and lanthanum-doped adsorbents at 303 K are shown in Fig. 1. The kinetic diameter of benzene is approximately 5.85 Å, which is calculated from the minimum equilibrium cross-sectional diameter [39], and it can therefore be easily adsorbed on the surface or inside the pore channel of prepared adsorbents. When initially using mesoporous TiO_2 as the adsorbent, the high slope of the breakthrough curve indicates very fast adsorption with a minimum mass transfer effect, 96% of the relative benzene concentration was obtained in the first 10 min, and subsequently reached a plateau easily after 30 min ($C = C_o$). As seen in Table 2, the corresponding adsorption capacity was quite low, approximately 7.75 μmol g$_{ads}$$^{-1}$. The incorporation of cerium and lanthanum species into a mesoporous framework remarkably promotes the benzene removal and the total experimental times were extended to 90–95 min. The adsorbed quantities increased with the lanthanide amount, and the 5.0Ce–TiO_2 and 5.0La–TiO_2 samples achieved the highest adsorption capacities, 37.17 μmol g$_{ads}$$^{-1}$ and 50.66 μmol g$_{ads}$$^{-1}$, respectively. Thus, the adsorption efficiency is affected by the lanthanide content in the adsorbent. For a comprehensive view, the evolution of specific surface area and adsorption

Table 1
Characteristics of all adsorbents corresponding to sorption measurements, XRD, and XPS analysis.

Adsorbents	Surface area ($m^2\,g^{-1}$)	Micropore area ($m^2\,g^{-1}$)	Pore volume ($cm^3\,g^{-1}$)	Pore size (nm)	Crystallite size (nm)	Oxidation states
TiO$_2$	35.77	–	0.0408	3.2582	17.58	Ti^{4+}, O$_I$, O$_{II}$
0.1Ce–TiO$_2$	53.31	1.98	0.1019	5.4679	14.35	Ti^{4+}, O$_I$, O$_{II}$
0.5Ce–TiO$_2$	77.83	3.87	0.1689	6.2334	10.65	Ti^{4+}, O$_I$, O$_{II}$
1.0Ce–TiO$_2$	79.08	5.78	0.1757	6.7335	13.79	Ti$^{3+/4+}$, Ce^{3+}, O$_I$, O$_{II}$
5.0Ce–TiO$_2$	94.49	10.02	0.2248	7.1461	8.68	Ti$^{3+/4+}$, Ce$^{3+/4+}$, O$_I$, O$_{II}$
10Ce–TiO$_2$	67.86	6.80	0.2762	12.5173	9.83	Ti$^{2+/3+/4+}$, Ce$^{3+/4+}$, O$_I$, O$_{II}$
0.1La–TiO$_2$	46.51	1.22	0.0791	4.8979	13.40	Ti^{4+}, O$_I$, O$_{II}$
0.5La–TiO$_2$	78.48	2.85	0.1466	5.4411	10.82	Ti^{4+}, O$_I$, O$_{II}$
1.0La–TiO$_2$	74.06	5.35	0.1593	6.3585	10.90	Ti^{4+}, La^{3+}, O$_I$, O$_{II}$
5.0La–TiO$_2$	105.66	10.55	0.2403	6.6097	8.57	Ti$^{3+/4+}$, La^{3+}, O$_I$, O$_{II}$
10La–TiO$_2$	74.93	8.43	0.3025	12.3434	9.44	Ti^{4+}, La^{3+}, O$_I$, O$_{II}$

behavior of xCe–TiO$_2$ and xLa–TiO$_2$ as a function of rare earth metal content at 303 K are illustrated in Fig. 2. The adsorptivity increases with metal content to reach a maximum at 5 mol% and then decreases with further doping. It is possible to correlate to either the BET specific surface area or microporous area of the adsorbents, but they are not proportional to the increase in doping. As seen in Table 1, no microporosity was observed for pure mesoporous titania whereas metal-doped samples possess bi-porous structure composing of both micro- and mesopores. Micropore areas increased averagely from 1.5 $m^2\,g^{-1}$ to 5.5 $m^2\,g^{-1}$ according to BET surface areas, as raising lanthanide content up to 1 mol%. 5.0Ce–TiO$_2$ and 5.0La–TiO$_2$ samples showed the highest micro-
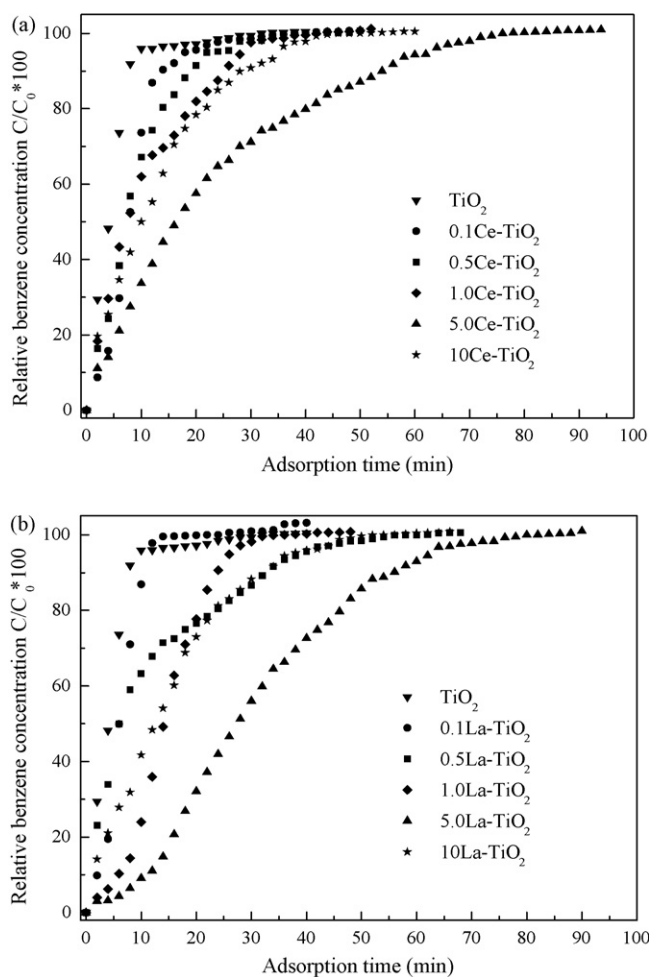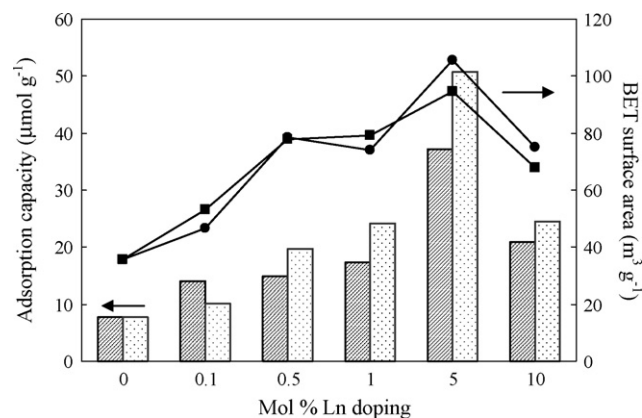

Fig. 2. Relationship between specific surface area and adsorption capacity of doped mesoporous adsorbents at 303 K: (▨) q_{Ce}, (▩) q_{La}, (■) S_{Ce} and (●) S_{La}.

porosity, 10.02 $m^2\,g^{-1}$ and 10.55 $m^2\,g^{-1}$, respectively. The higher framework microporosity leads to higher pore filling or stronger interaction between the adsorbents and gas molecules, therefore, resulting in the gradual enhancement in benzene-adsorbed amount up to the optimal capacity of 5.0Ln–TiO$_2$. Nevertheless, 10 mol% doped samples displayed 20% diminution of micropore area due to the decrease in specific surface area and increase in pore diameter aforementioned, corresponding to the reduction in adsorptivity. These results are consistent with numerous reported literatures on bi-porous materials irrespective of light hydrocarbon, aliphatic or aromatic hydrocarbons [40–44]. The microporosity also influences on the adsorption behavior for gaseous benzene via the relative diffusion control. The breakthrough curves in Fig. 1 significantly indicated the faster diffusion for either smaller mesopores or micropores samples. Typically, the uptake curves of TiO$_2$ and 0.1Ln–TiO$_2$ easily achieved the flat plateau regions within 30 min. It is realized that the diffusivities increased according to the relative micropore

Fig. 1. Breakthrough curves for benzene adsorption at 303 K on (a) xCe–TiO$_2$ and (b) xLa–TiO$_2$.

Table 2
Adsorption capacity of benzene on xCe–TiO$_2$ and xLa–TiO$_2$ at 303 K and 343 K.

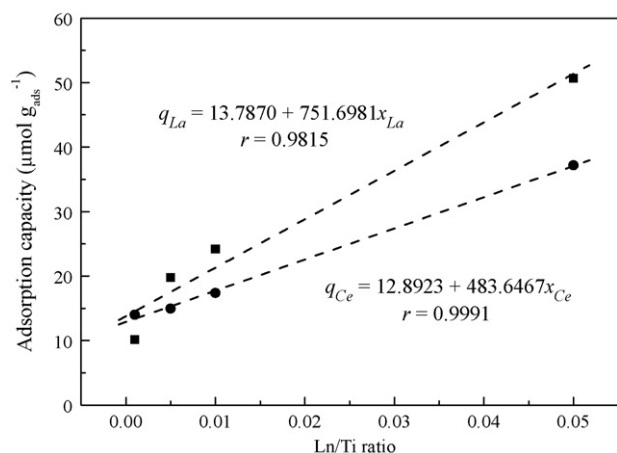| Adsorbents	Ln/Ti ratio	Benzene amount (μmol g$_{ads}^{-1}$)	
		@ 303 K	@ 343 K
TiO$_2$	0.000	7.75	1.95
0.1Ce–TiO$_2$	0.001	14.00	3.74
0.5Ce–TiO$_2$	0.005	14.95	6.28
1.0Ce–TiO$_2$	0.010	17.37	5.73
5.0Ce–TiO$_2$	0.050	37.17	20.35
10Ce–TiO$_2$	0.100	20.85	2.54
0.1La–TiO$_2$	0.001	10.15	2.32
0.5La–TiO$_2$	0.005	19.75	3.35
1.0La–TiO$_2$	0.010	24.20	2.89
5.0La–TiO$_2$	0.050	50.66	17.62
10La–TiO$_2$	0.100	24.44	2.79

Fig. 3. Adsorption capacity (q) as a function of lanthanide dosage in a range of 0.1 and 5 mol%.

area; and the slowest diffusion was attained for 5Ln–TiO$_2$ samples which contained the highest values of approximate 10 m^2 g^{-1}. Otherwise, the partial collapse of mesostructure in case of the excess lanthanide amount, as previously suggested via the evidence from N$_2$ adsorption/desorption measurement [38], indispensably hindered the diffusion of benzene molecules. However, once again, the microporous regions dominated the adsorbability in view of the reduction in micropore areas, resulting in the faster diffusion and the corresponding lower benzene-adsorbed amounts than those of 5 mol% doped materials. It obviously indicated that the framework microporosity plays an important role in controlling diffusion mechanism of the adsorbate molecules over bi-porous materials directly relating to the adsorbability. Similar observations were also acknowledged by Hoang et al. [43,45] and Huang et al. [44]. Associating several parameters, such as the largest external surface area and micropore area, high total pore volume and pore diameter, 5 mol% lanthanide doping content is the optimum amount for the adsorption conditions in the present study.

The relationship of the adsorption capacity to lanthanide dosages between 0.1 and 5 mol% is determined in Fig. 3. The adsorbed benzene increased linearly as the doping percentage increased to 5 mol%, with high correlation coefficients (r) of 0.9991 and 0.9815 for cerium and lanthanum, respectively, corresponding to the following equations:

$$q_{Ce} = 12.8923 + 483.6467x_{Ce}$$

$$q_{La} = 13.7870 + 751.6981x_{La}$$

Correspondingly, the higher Ln/Ti ratio results in larger surface area and microporous area, and greater adsorption capacity of benzene on account of more accessible space for the aromatic adsorbate to accumulate and adsorb on the surface or inside the mesoporous adsorbent. However, benzene saturation capacities decreased to half at 10 mol%, approximately 20.85 μmol g$_{ads}^{-1}$ (10Ce–TiO$_2$) and 24.44 μmol g$_{ads}^{-1}$ (10La–TiO$_2$) due to the reduction in both the external surface area and micropore area, even though the higher pore volume and larger pore size were observed (~0.3 cm^3 g^{-1} and 12.0 nm). In addition, the immoderate metal contents are detrimental, producing partially collapsed mesostructures or conducting to a portion of lanthanide that does not work as an active adsorption site and likely hindering benzene adsorbability [38]. Accordingly, the textural properties are significant factors that influence the adsorption capacity of adsorbents. The increase in specific surface area, which corresponds to the amount of surface hydroxyl groups, may lead to a greater number of gas molecules adsorbed on the

adsorbents. Obviously, all lanthanum-doped samples exhibit much better adsorptive characteristics than cerium-doped samples, especially at higher dosages, which could be ascribed to the complicated existence of Ce and Ti chemical states in cerium-doped samples that correlate to the generation of active sorption sites in the mesostructure framework.

Alternatively, the adsorption performance is strongly connected to the interaction between benzene and surface hydroxyl groups (–OH), as well as the specific interaction between the gaseous adsorbate and the active cation sites or the electron-transfer process between the aromatic adsorbate and metal-oxide substrate. Moreover, the steric factor may also have an impact on the adsorption behavior. A detailed explanation or prediction will be discussed afterwards in order to highlight the adsorption behavior of benzene on rare earth doped mesoporous TiO$_2$.

3.3. Effect of temperature on the adsorption of benzene

Benzene removal at 343 K was also conducted to investigate the effect of adsorption temperature on the performance of mesoporous adsorbents. The experimental results summarized in Table 2 indicate that 1.95 μmol g$_{ads}^{-1}$ of benzene was adsorbed on the surface of the un-doped sample. 97.3% of the relative benzene concentration was achieved after only 2 min, and the increase to saturation was much faster, within 16 min. Moreover, according to the experimental breakthrough curves presented in Fig. 4, the
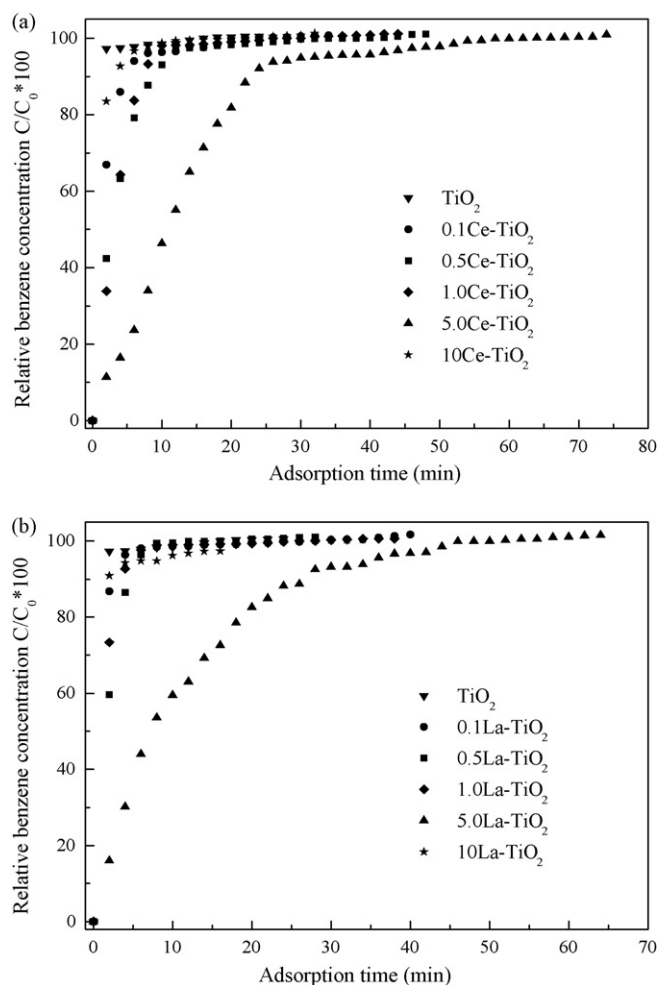

Fig. 4. Breakthrough curves for benzene adsorption at 343 K on (a) xCe–TiO$_2$ and (b) xLa–TiO$_2$.

lanthanide dopants show slightly positive effects on the adsorption capacity, similar to the results at 303 K; increasing metal leads to an increase in adsorbed benzene. One hundred percent of the relative benzene concentrations on both cerium- and lanthanum-doped mesoporous titania was reached after 25-35 min. 5.0Ce–TiO$_2$ and 5.0La–TiO$_2$ offer the highest adsorption capacities for benzene, 20.35 and 17.62 μmol g$_{ads}^{-1}$, respectively, after 60–70 min. These results are attributed to the external and micropore surface area of all of the adsorbents concerned above. The linear correlations between q and x were in the range of 0.1 and 5 mol% doping, with acceptable r values, 0.9928 and 0.9897, respectively, corresponding to the following equations:

$$q_{Ce} = 3.5040 + 334.6064x_{Ce}$$

$$q_{La} = 1.2096 + 323.3572x_{La}$$

Thus, as shown in Fig. 5, contrary to the adsorption at 303 K, the two linear fittings of parallel cerium-doped samples show adsorbability better than those of lanthanum. It can be concluded that the benzene-adsorbed quantity is enhanced with respect to the increase in dopant dosage, regardless of the adsorption temperature. Unfortunately, the excess lanthanide is considered to inhibit the benzene adsorbability similarly to those at 303 K, only 2.54 μmol g$_{ads}^{-1}$ for 10Ce–TiO$_2$ and 2.79 μmol g$_{ads}^{-1}$ for 10La–TiO$_2$. Accordingly, a drastic reduction of adsorbed amounts was observed at higher temperature on lanthanide-doped samples. Typically, 50–70% of benzene adsorption capacity was diminished as the cerium content was up to 1 mol%, whereas those was 10–25% for xLa–TiO$_2$. The results imply the more significant impact of temperature on the adsorption behavior of cerium dopant than that of lanthanum in case of low metal concentrations. 45% and 65% declination of adsorbed quantity were recorded with the optimum cerium and lanthanum loading, respectively. However, approximately 88% of adsorptivity was reduced for 10 mol% samples compared to those at 303 K.

Generally, a decrease in adsorbed benzene on metal-doped mesoporous TiO$_2$ at higher temperature implies that benzene molecules are weakly adsorbed to the adsorbents. The rapid and strong collision at 343 K could lead to shorter contact time and weaker interaction between the aromatic gas molecule and adsorption site on the surface, thus limiting the adsorption tendency.
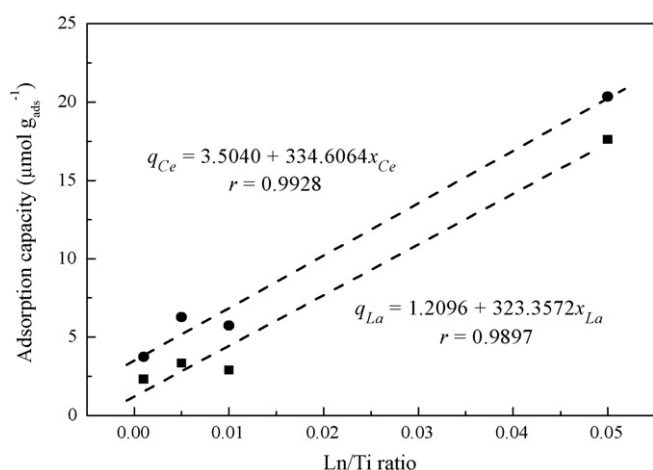

Fig. 5. Adsorption capacity for benzene at 343 K with various Ln/Ti ratio.

3.4. Adsorption behavior of benzene molecules and mesostructured adsorbent

As mentioned before, the adsorption of gaseous benzene on rare earth metal-doped mesoporous titania possibly follows the physical route and depends remarkably on the textural characteristics of adsorbents. The adsorbability enhances with metal content due to the higher mesoporosity and microporosity, a typically larger surface area, micro area, pore volume, and pore diameter, and thus higher diffusivities and more accessibility of gas molecules. The incorporation of rare earth metal into the framework induces a modification in benzene adsorptivity. However, the excess of lanthanide leads to a reduction of adsorbed benzene due to the decrease in either surface area or microporous area. According to the results, 5 mol% lanthanide is the optimal doping amount for benzene adsorptivity and for ensuring higher benzene adsorption on lanthanum-doped mesoporous TiO$_2$ adsorbents, making it more effective than cerium-doped adsorbents at 303 K because of a larger BET specific surface area.

Furthermore, the hydroxyl groups at the outmost surface of the adsorbent or in the wall of the pore channel are of considerable importance for determining the physico-chemical characteristics and correlation to the adsorption performance. The adsorption behavior may be attributed to the adsorbent–adsorbate interaction, essentially predominated by the interaction between the surface hydroxyl or titanol groups of mesoporous walls and aromatic rings. Similar to the mesoporous silicate, the surfaces of pure and metal-doped mesoporous TiO$_2$ are abundant in hydroxyl groups, which behave as acidic sites according to the classification of Kiselev and Yashin [46] and Davydov [47], and be found as isolated M–OH groups (monodentate sites) and geminal M–(OH)$_2$ groups (bidentate sites), where M is a metal. Considering the molecular orbitals of benzene, benzene is strongly attached to the adsorbent surface via an OH–π bonding interaction from the three π bonds and the three sp^2-orbital and six p$_z$-orbitals in the ring. Therefore, the adsorbability is partially dependent on the nature of these OH groups, viz. either the type or amount of available surface hydroxyl groups. McCafferty and Wightman [48] as well as Meng et al. [49] experimentally determined that the average content of surface hydroxyl groups was approximately 11 OH nm^{-2} for titanium dioxide anatase. Correspondingly, the better adsorptivity might be predicted by the higher number of OH groups or the generation of more acidic sites when incorporating altervalent metal ions in the mesostructure network.

Alternatively, adsorbability was also influenced by the chemical structure of their surface, typically the existence of an oxidation state of a different metal ion in the matrix, pore channel, or on the surface. According to the XPS results [38], cerium-doped samples at low metal content, indicated only Ti^{4+}, O^{2-}, OH/adsorbed H$_2$O and trace Ce^{3+} and thus, the physico-chemical properties as well as the interaction between surface OH and benzene may dominate the adsorption performance at 303 K. As the cerium amount increased to 5 mol%, the increases in coordinatively unsaturated Ti^{3+}, Ce$^{3+/4+}$, oxygen deficiencies and oxygen lattice of Ti–O, Ce–O, Ce–O–Ti increased because of the reduction of Ti^{4+}. Additionally, the oxidation of Ce^{3+} combined with electron transfer and charge imbalance, contributes to benzene adsorbability in addition to the physical characteristics. Indeed, the electronic configurations of Ti^{3+} and Ce^{3+} are 1s^{2}2s^{2}2p^{6}3s^{2}3p^{6}4s^1(3d^0) and 1s^{2}2s^{2}2p^{6}3s^{2}3p^{6}4s^{2}3d^{10}4p^{6}5s^{2}4d^{10}5p^{6}4f^1(5d^{0}6s^0), respectively, whereas the saturated outer shells were found for either Ti^{4+} or Ce^{4+}. When benzene interacts with the adsorbent, the π-orbital of benzene can overlap with the unfilled or vacant outer shell s-orbital of Ti^{3+} to form a σ-bond (σ donation) or overlap with the unfilled f-orbital of Ce^{3+}, although it may be improbable for cerium. Moreover, the back-donation of electron charges from the

d-orbital of the metal to the antibonding π^* of benzene, known as d-π^* back-donation, might appear, and effect adsorption behavior. Therefore, the 5.0Ce–TiO$_2$ sample exhibits the best benzene adsorption capacity. Nevertheless, the slight increase in Ce^{3+}, Ti$^{2+/4+}$ and lattice oxygen in Ce$_{10}$TiO$_2$, accompanied by the decline of Ce^{4+}, Ti^{3+} and OH/adsorbed H$_2$O can result in less σ donation and d-π^* back-donations. Together with these interactions, the reduction in specific surface area with immoderate doping plays a dominant role in the adsorbability of benzene; the smaller the accessible area, the worse the adsorbed quantity.

On the contrary, almost no alterations in the XPS spectra with corresponding lanthanum [38] were observed with octa-hedrally coordinated Ti^{4+}, La^{3+}, lattice oxygen Ti–O and surface OH groups. In these cases, the adsorption behavior at 303 K is influenced strongly by the physico-chemical characteristics of adsorbent and the interaction between the surface OH group and π-electron of benzene as discussed earlier. Accordingly, the adsorption capacity for benzene increases with respect to the specific surface area. The electronic configuration of La^{3+} is $1s^2 2s^2 2p^6 3s^2 3p^6 4s^2 3d^{10} 4p^6 5s^2 4d^{10} 5p^6 (6s^0 5d^0 4f^0)$, and therefore the d-$\pi^*$ back-donation between lanthanum and benzene may occur in all samples. The exception was found only for 5.0La–TiO$_2$, with the highest adsorption capacity for benzene in the presence of tetrahedral Ti^{3+} with the unfilled s-orbital in the outer shell, resulting in σ-donation.

4. Conclusions

In this study, the presence of different cerium and lanthanum amounts significantly promoted the adsorption capacity of benzene compared to un-doped samples. The loading of rare earth metal is an important parameter because of its direct effect on either physical characteristics or the chemical properties of samples. Adsorptivity increases with lanthanide doping to reach a maximum at 5 mol% and then decreases with immoderate amounts. Moreover, temperature also remarkably affects adsorbability with a 70–90% decrease, implying the weak physisorption of benzene on the adsorbents. 5.0Ce–TiO$_2$ and 5.0La–TiO$_2$ exhibited the highest benzene-adsorbed quantity, irrespective of reaction temperature. The adsorption behavior could be attributed to the specific surface area and micropore area of the adsorbent, the provision of more acidic sites, OH-π-electron interaction, and the formation of σ-bonding and d-π^* back-donation between benzene and mesostructured adsorbents.

Acknowledgment

References

[1] USEPA (Environmental Protection Agency), Reducing Risk: Setting Priorities and Strategies for Environmental Protection, US Environmental Protection Agency, Washington D.C., 1990 (EPA-SAB-EC-90-021).

[2] USEPA (Environmental Protection Agency), A comparison of indoor and outdoor concentrations of hazardous air pollutants, in: Inside IAQ, Spring/Summer 1998, Office of Research and Development, U.S. Environmental Protection Agency, Research Triangle Park, NC, 1998, pp. 1–7 (EPA/600/N-98/002).

[3] M.O. Bachmann, J.E. Myers, Influences on sick building syndrome symptoms in three buildings, Soc. Sci. Med. 40 (1995) 245–251.

[4] K. Chang, C. Lu, M.-R. Lin, Treatment of volatile organic compounds from polyurethane and epoxy manufacture by a trickle-bed air biofilter, J. Biosci. Bioeng. 92 (2001) 126–130.

[5] H. Ichiura, T. Kitoka, H. Tanaka, Removal of indoor pollutants under UV irradiation by a composite TiO$_2$-zeolite sheet prepared using a papermaking technique, Chemosphere 50 (2003) 79–83.

[6] J.-P. Bellat, M.-H. Simonot-Grange, S. Jullian, Adsorption of gaseous p-xylene and m-xylene on NaY, KY and BaY zeolites: Part 1. Adsorption equilibria of pure xylenes, Zeolites 15 (1995) 124–130.

[7] D.P. Serrano, G. Calleja, J.A. Botas, F.J. Gutierrez, Adsorption and hydrophobic properties of mesostructured MCM-41 and SBA-15 materials for volatile organic compound removal, Ind. Eng. Chem. Res. 43 (2004) 7010–7018.

[8] B.D. Crittenden, W.J. Thomas, Adsorption Technology and Design, Butterworth-Heinemann, Linacre House, Jordan Hill, Oxford, 1998.

[9] Y.-C. Chiang, P.-C. Chiang, C.-P. Huang, Effects of pore structure and temperature on VOC adsorption on activated carbon, Carbon 39 (2001) 523–534.

[10] C.-M. Wang, K.-S. Chang, T.-W. Chung, Adsorption equilibria of aromatic compounds on activated carbon, silica gel and 13X zeolite, J. Chem. Eng. Data 49 (2004) 527–531.

[11] A.K. Nowak, C.J.J. Den Ouden, S.D. Pikett, B. Smit, A.K. Cheetham, M.F.M. Post, Mobility of adsorbed species in zeolites: methane, ethane and propane diffusivities, J. Phys. Chem. 95 (1991) 848–854.

[12] P.S. Chintawar, H.L. Greene, Adsorption and catalytic destruction of trichloroethylene in hydrophobic zeolites, Appl. Catal. B: Environ. 14 (1997) 37–47.

[13] P.A. Sewell, A.M. Morgan, Methanol vapor adsorption on silica and soda-lime-silica glass, J. Am. Ceram. Soc. 52 (1969) 136–138.

[14] W. Pohle, Infrared study of the adsorption of aromatic molecules onto silica and chlorinated silica. Application of the charge-transfer theory to the date, J. Chem. Soc. Faraday Trans. 1 (78) (1982) 2101–2109.

[15] E. Papirer, Adsorption on silica surfaces Surfactant Science Series, vol. 90, Marcel Dekker Inc., New York, 2000.

[16] S. Carlos-Cuellar, P. Li, A.P. Christensen, B.J. Krueger, C. Burrichter, V.H. Grassian, Heterogeneous uptake kinetics of volatile organic compounds on oxide surfaces using a Knudsen cell reactor: adsorption of acetic acid, formaldehyde, and methanol on α-Fe$_2$O$_3$, α-Al$_2$O$_3$, and SiO$_2$, J. Phys. Chem. A 107 (2003) 4250–4261.

[17] H. Zaitan, D. Bianchi, O. Achak, T. Chafik, A comparative study of the adsorption and desorption of o-xylene onto bentonite clay and alumina, J. Hazard. Mater. 153 (2008) 852–859.

[18] C.T. Kresge, M.E. Leonowicz, W.J. Roth, J.C. Vartuli, J.S. Beck, Ordered mesoporous molecular sieves synthesized by a liquid-crystal template mechanism, Nature 359 (1992) 710–712.

[19] D. Zhao, Q. Huo, J. Feng, B.F. Chmelka, G.D. Stucky, Nonionic triblock and star diblock copolymer and oligomeric surfactant syntheses of highly ordered, hydrothermally stable, mesoporous silica structures, J. Am. Chem. Soc. 120 (1998) 6024–6036.

[20] G. Øye, J. Sjöblom, M. Stöcker, Synthesis and characterization of siliceous and aluminum-containing mesoporous materials from different surfactant solutions, Micropor. Mesopor. Mater. 27 (1999) 171–180.

[21] Y.-H. Chu, H.-J. Kim, K.-Y. Song, Y.-G. Shul, K.-T. Jung, K. Lee, M.-H. Han, Preparation of mesoporous silica fiber matrix for VOC removal, Catal. Today 74 (2002) 249–256.

[22] E.W. Shin, J.S. Han, M. Jang, S.-H. Min, J.K. Park, R.M. Rowell, Phosphate adsorption on aluminum-impregnated mesoporous silicates: surface structure and behavior of adsorbents, Environ. Sci. Technol. 38 (2004) 912–917.

[23] R. Serna-Guerrero, A. Sayari, Applications of pore-expanded mesoporous silica. 7. Adsorption of volatile organic compounds, Environ. Sci. Technol. 41 (2007) 4761–4766.

[24] T.-D. Nguyen-Phan, C.Y. Lee, J.S. Chung, E.W. Shin, Adsorption of benzene onto mesoporous silicates modified by titanium, Res. Chem. Intermed. 34 (2008) 743–753.

[25] D.M. Antonelli, J.Y. Ying, Synthesis of hexagonally packed mesoporous TiO$_2$ by a modified sol–gel method, Angew. Chem. Int. Ed. Engl. 34 (1995) 2014–2017.

[26] Z.R. Tian, W. Tong, J.Y. Wang, N.G. Duan, V.V. Krishnan, S.L. Suib, Manganese oxide mesoporous structures: mixed-valent semiconducting catalysts, Science 276 (1997) 926–930.

[27] S. Banerjee, A. Santhanam, A. Dhathathreyan, P.M. Rao, Synthesis of ordered hexagonal mesostructured nickel oxide, Langmuir 19 (2003) 5522–5525.

[28] A.K. Sinha, S. Seelan, S. Tsubota, M. Haruta, A three-dimensional mesoporous titanosilicate support for gold nanoparticles: vapor-phase epoxidation of propene with high conversion, Angew. Chem. 116 (2004) 1572–1574;
A.K. Sinha, S. Seelan, S. Tsubota, M. Haruta, A three-dimensional mesoporous titanosilicate support for gold nanoparticles: vapor-phase epoxidation of propene with high conversion, Angew. Chem. Int. Ed. 43 (2004) 1546–1548.

[29] X. Chen, S.S. Mao, Titanium dioxide nanomaterials: synthesis, properties, modifications and applications, Chem. Rev. 107 (2007) 2891–2959.

[30] V.F. Stone Jr., R.J. Davis, Synthesis, characterization, and photocatalytic activity of titania and niobia mesoporous molecular sieves, Chem. Mater. 10 (1998) 1468–1474.

[31] J.C. Yu, L. Zhang, J. Yu, Rapid synthesis of mesoporous TiO$_2$ with high photocatalytic activity by ultrasound-induced agglomeration, New J. Chem. 26 (2002) 416–420.

[32] I. Kartini, P. Meredith, J.C. Diniz Da Costa, G.Q. Lu, A novel route to the synthesis of mesoporous titania with full anatase nanocrystalline domains, J. Sol–Gel Sci. Tech. 31 (2004) 185–189.

[33] M.D. Pérez, E. Otal, S.A. Bilmes, G.J.A.A. Soler-Illia, E.L. Crepaldi, D. Grosso, C. Sanchez, Growth of gold nanoparticle arrays in TiO$_2$ mesoporous matrixes, Langmuir 20 (2004) 6879–6886.

[34] G. Liu, Y. Zhao, C. Sun, F. Li, G.Q. Lu, H.-M. Cheng, Synergistic effects of B/N doping on the visible-light photocatalytic activity of mesoporous TiO$_2$, Angew. Chem. Int. Ed. 47 (2008) 1–6.

[35] Y.-H. Zhang, A. Reller, Nanocrystalline iron-doped mesoporous titania and its phase transition, J. Mater. Chem. 11 (2001) 2537–2541.

[36] H. Yoshitake, Y. Aoki, S. Hemmi, Mesoporous titania supported-molybdenum catalysts: the formation of a new mesophase and use in ethanol–oxygen catalytic reactions, Micropor. Mesopor. Mater. 93 (2006) 294–303.

[37] Y. Izumi, K. Konishi, D.M. Obaid, T. Miyajima, H. Yoshitake, X-ray absorption fine structure combined with X-ray fluorescence spectroscopy. Monitoring of vanadium sites in mesoporous titania, excited under visible light by selective detection of vanadium $K\beta_{5,2}$ fluorescence, Anal. Chem. 79 (2007) 6933–6940.

[38] T.-D. Nguyen-Phan, M.B. Song, E.J. Kim, E.W. Shin, The role of rare-earth metals in lanthanide-doped mesoporous titania, Micropor. Mesopor. Mater. 119 (2009) 290–298.

[39] D.W. Breck, Zeolite Molecular Sieves—Structure, Chemistry and Use, Wiley, New York, 1974.

[40] B.L. Newalkar, N.V. Choudary, P. Kumar, S. Komarneni, T.S.G. Bhat, Exploring the potential of mesoporous silica, SBA-15, as an adsorbent for light hydrocarbon separation, Chem. Mater. 14 (2002) 304–309.

[41] B.L. Newalkar, N.V. Choudary, U.T. Turaga, R.P. Vijayalakshmi, P. Kumar, S. Komarneni, T.S.G. Bhat, Potential adsorbent for light hydrocarbon separation: role of SBA-15 framework porosity, Chem. Mater. 15 (2003) 1474–1479.

[42] F.B. Li, X.Z. Li, C.H. Ao, S.C. Lee, M.F. Hou, Enhanced photocatalytic degradation of VOCs using Ln^{3+}-TiO_2 catalysts for indoor air purification, Chemosphere 59 (2005) 787–800.

[43] V.-T. Hoang, Q. Huang, M. Eić, T.-O. Do, S. Kaliaguine, Structure and diffusion characterization of SBA-15 materials, Langmuir 21 (2005) 2051–2057.

[44] Q. Huang, V.-T. Hoang, A. Malekian, M. Eić, T.-O. Do, S. Kaliaguine, Adsorption of *n*-heptane, toluene and *o*-xylene on mesoporous UL-ZSM-5 materials, Micropor. Mesopor. Mater. 87 (2006) 224–234.

[45] V.-T. Hoang, Q. Huang, A. Ungureanu, M. Eić, T.-O. Do, S. Kaliaguine, Structure and diffusion characterizations of steam-stable mesostructured zeolitic UL-ZSM-5 materials, Langmuir 22 (2006) 4777–4786.

[46] A.V. Kiselev, Y.I. Yashin, Gas-chromatographic determination of adsorption and specific surface for solids, in: Gas Adsorption Chromatography, Plenum Press, New York, 1969, pp. 104–145.

[47] A. Davydov, Molecular spectroscopy of oxide catalyst surfaces, John Wiley, New York, 2003.

[48] E. McCafferty, J.P. Wightman, Determination of the concentration of surface hydroxyl groups on metal oxide films by a quantitative XPS method, Surf. Interface Anal. 26 (1998) 549–564.

[49] X.G. Meng, M. Dadachov, G.P. Korfiatis, C. Christodoulatos, Methods of preparing a surface-activated titanium oxide product and of using same in water treatment processes, US Patent 6,919,029 (2005).